SIAM J. SCI. COMPUT.
Vol. 44, No. 5, pp. A2918–A2943

A CONTINUATION MULTIPLE SHOOTING METHOD FOR WASSERSTEIN GEODESIC EQUATION*

JIANBO CUI†, LUCA DIECI‡, AND HAOMIN ZHOU‡

Abstract. In this paper, we propose a numerical method to solve the classic L^2-optimal transport problem. Our algorithm is based on the use of multiple shooting, in combination with a continuation procedure, to solve the boundary value problem associated to the transport problem. Based on the viewpoint of Wasserstein Hamiltonian flow with initial and target densities, our algorithm reflects the Hamiltonian structure of the underlying problem and exploits it in the numerical discretization. Several numerical examples are presented to illustrate the performance of the method.

Key words. Hamiltonian flow, boundary value problem, optimal transport, multiple shooting method

MSC codes. 49Q22, 49M25, 65L09, 34A55

DOI. 10.1137/21M142160X

1. Introduction.

Optimal transport (OT) has a long and rich history, and it finds applications in various fields, such as image processing, machine learning, and economics (e.g., see [22, 29]). The first mass transfer problem, a civil engineering problem, was considered by Monge in 1781. A modern treatment of this problem, in terms of probability densities, was studied by Kantorovich in [18]. In this light, the OT problem consists of moving a certain probability density into another, while minimizing a given cost functional. Depending on whether (one or both of) the densities are continuous or discrete, we have a fully discrete, or a semidiscrete, or a continuous OT problem. In this work, we consider a continuous OT problem subject to the cost given by the squared L^2 norm. This is the most widely studied continuous OT problem, and the formulation we adopt in this paper is based on an optimal control formulation in a fluid mechanics framework, known as the *Benamou–Brenier formula*, established in [3]. The starting point is to cast the OT problem in a variational form as

$$\inf_{v} \left\{ \int_0^1 \langle v, v\rangle_\rho dt \ : \ \partial_t \rho + \nabla \cdot (\rho v) = 0, \rho(0) = \mu, \rho(1) = \nu \right\}, \tag{1.1}$$

where $\langle v, v\rangle_\rho := \int_{\mathbb{R}^d} |v|^2 \rho dx$ with smooth velocity field $v(t,x) \in \mathbb{R}^d$, and μ and ν are probability density functions satisfying $\int_{\mathbb{R}^d} |x|^2 \mu(x) dx, \int_{\mathbb{R}^d} |x|^2 \nu(x) dx < +\infty$. This ensures the existence and uniqueness of the optimal map M^* for the equivalent Monge–Kantorovich problem of (1.1), i.e., $\inf_M \int_{\mathbb{R}^d} |M(x) - x|^2 \mu(x) dx$ with

*Submitted to the journal's Methods and Algorithms for Scientific Computing section May 21, 2021; accepted for publication (in revised form) April 18, 2022; published electronically September 12, 2022.

https://doi.org/10.1137/21M142160X

Funding: This research was partially supported by the Georgia Tech Mathematics Application Portal (GT-MAP) and by research grants NSF DMS-1620345, NSF DMS-1830225, and ONR N00014-18-1-2852. The research of the first author was partially supported by the Hong Kong Research Grant Council ECS grant 25302822, internal funds P0039016 and P0041274 from The Hong Kong Polytechnic University, and the CAS AMSS-PolyU Joint Laboratory of Applied Mathematics.

†Corresponding author. School of Mathematics, Georgia Institute of Technology, Atlanta, GA 30332 USA (jcui82@math.gatech.edu). Current address: Department of Applied Mathematics, The Hong Kong Polytechnic University, Hung Hom, Kowloon, Hong Kong (jianbo.cui@polyu.edu.hk).

‡School of Mathematics, Georgia Institute of Technology, Atlanta, GA 30332 USA (luca.dieci@math.gatech.edu, hmzhou@math.gatech.edu).

$M : \mathbb{R}^d \to \mathbb{R}^d$ transferring μ to ν (see, e.g., [29, Theorem 1.22]). Moreover, the optimal map has the form $M^*(x) = \nabla\psi(x) = x + \nabla\phi(x)$, μ-a.s., with a convex function $\psi(x)$. From [3], we have that $\nabla\phi(x) = v(0,x)$ and that the characteristic line $(X(t,x), v(t,X(t,x)))$ satisfies

$$\partial_t\rho(t,X(t,x)) + \nabla\cdot(\rho(t,X(t,x))v(t,X(t,x))) = 0,$$
$$\partial_t v(t,X(t,x)) + \nabla\Big(\frac{1}{2}|v(t,X(t,x))|^2\Big) = 0.$$

When $X(t,x) = x + tv(0,x)$ is invertible, we obtain that $\rho(t) = X(t,\cdot)^{\#}\rho(0)$ and that $v(t,x) = v(0,X^{-1}(t,x)) = \nabla\psi(0,X^{-1}(t,x))$. We refer to [5, 15, 29] and references therein for results about regularity of M^* and ψ. The optimal value in (1.1) is known as the L^2-Wasserstein distance square between μ and ν, and written as $g_W^2(\mu,\nu)$. The formulation (1.1) is interpreted as finding the optimal vector field v to transport the given density function μ to the density ν with the minimal amount of kinetic energy. (We emphasize that the "time variable" t has no true physical meaning, and it serves the role of a homotopy parameter.)

An alternative viewpoint for solving the minimization problem (1.1) is via the Hamiltonian flow on the density manifold (see, e.g., [9, 11]). More precisely, by considering the Lagrange multiplier technique, we can look for the critical point (ρ, v, λ) of the following:

$$\mathcal{L}(v,\rho,\lambda) := \int_0^1\int_{\mathbb{R}^d} |v(t,x)|^2\rho(t,x)dtdx + \int_0^1\int_{\mathbb{R}^d} \lambda(t,x)(\partial_t\rho(t,x) + \nabla\cdot(\rho(t,x)v(t,x)))dtdx.$$

Taking the variational derivative with respect to ρ, v, λ and using integration by parts, we obtain, respectively,

$$\frac{\delta\mathcal{L}}{\delta\rho} = |v(t,x)|^2 - \partial_t\lambda(t,x) - v(t,x)\cdot\nabla v(t,x),$$
$$\frac{\delta\mathcal{L}}{\delta v} = 2v(t,x)\rho(t,x) - \nabla\lambda(t,x)\rho(t,x),$$
$$\frac{\delta\mathcal{L}}{\delta\lambda} = \partial_t\rho(t,x) + \nabla\cdot(\rho(t,x)v(t,x)).$$

Thus the critical point of $\mathcal{L}$ satisfies the following equations:

$$(2v(t,x) - \nabla\lambda(t,x))\rho(t,x) = 0,$$
$$|v(t,x)|^2 - \partial_t\lambda(t,x) - v(t,x)\cdot\nabla\lambda(t,x) = 0,$$
$$\partial_t\rho(t,x) + \nabla\cdot(\rho(t,x)v(t,x)) = 0.$$

As a consequence, when $\rho(t,x)$ remains positive, letting $S(t,x) = \frac{1}{2}\lambda(t,x)$ (namely $v(t,x) = \nabla S(t,x)$), we obtain (up to a spatially independent function $C(t)$) the following system in the unknowns (ρ, S):

$$\begin{cases}\partial_t\rho + \nabla\cdot(\rho\nabla S) = 0,\\ \partial_t S + \frac{1}{2}|\nabla S|^2 = 0,\end{cases} \tag{1.2}$$

subject to boundary conditions $\rho(0) = \mu, \rho(1) = \nu$. If $S^0 = S\big|_{t=0}$ is known, the optimal value $g_W(\mu,\nu)$, the L^2-Wasserstein distance between μ and ν, equals $\sqrt{2H(\mu,S^0)}$

with $H(\rho, S) = \int_{\mathbb{R}^d} \frac{1}{2}|\nabla S|^2 \rho dx$. Our approach in solving the OT problem is to find some initial S^0 (or $v(0,x)$) such that the trajectory starting at (μ, S^0) passes through ν at $t = 1$. This is the well-known geodesic equation between two densities μ and ν on the Wasserstein manifold [31], and can also be viewed as a Wasserstein Hamiltonian flow with the Hamiltonian $H(\rho, S)$ [9].

Remark 1.1. Obviously, S is defined only up to an arbitrary constant. As a consequence, the (ρ, S) formulation (1.2) of the boundary value problem cannot have a unique solution. Because of this fact, we will in the end revert to using a formulation based on ρ and v, but the Hamiltonian structure of (1.2) will guide us in the development of appropriate semidiscretizations of the problem in the (ρ, v) variables.

In recent years, there have been several numerical studies concerned with approximating solutions of OT problems, and many of them are focused on the continuous problem considered in this work, that is, on computation of the Wasserstein distance g_W and the underlying OT map. A key result in this context is that the optimal map is the gradient of a convex function u, which is the solution of the so-called Monge–Ampére equation, a nonlinear elliptic PDE subject to nonstandard boundary conditions. We refer to [2, 4, 14, 17, 24, 27, 32] for a sample of numerical work on the solution of the Monge–Ampére equation. For different approaches, in the case of continuous, discrete, and semidiscrete OT problems, and for a variety of cost functions, we refer to [6, 12, 13, 21, 23, 25, 28, 30]. For instance, by adding a small Fisher information regularization term into the dynamical setting of the Benamou–Brenier formula, an optimization method was proposed in [21] to approximate the OT distance. In [28], a first-order primal-dual method was presented to solve the vector and matrix optimal mass transport. In [26], the authors introduced a family of numerical schemes based on entropic regularization and Sinkhorn's algorithm to approximate the OT problem in the Kantorvich formulation. Recently, several aspects of numerical methods, such as discretization of the forward-backward stochastic system and optimization techniques for variational problem in order to solve the discrete mean field game and mean field control problem, have been discussed in [20].

However, numerical approximation to the solution of the Wasserstein geodesic equation, a two-point boundary value problem, has not been directly considered in the existing literature. This is our main goal in the present paper. There are good reasons to consider solving the geodesic equation: at once, one can recover the Wasserstein distance, the OT map, and the "time dependent" vector field producing the optimal trajectory. At the same time, there are also a number of obstacles that make the numerical solution of the Wasserstein geodesic equation very challenging: the density ρ needs to be nonnegative, mass conservation is required, and retaining the underlying symplectic structure is highly desirable, too. Another hurdle, which is not at all obvious, is that the Hamiltonian system (1.2) with initial values on the Wasserstein manifold often develops singularities in finite time (see, e.g., [10]). These challenges must be overcome when designing numerical schemes for the boundary value problem (1.2).

In this paper, we propose computing the solution of (1.2) by combining a multiple shooting method, in conjunction with a continuation strategy, for an appropriate semidiscretization of (1.2). First, we consider a spatially discretized version of (1.2), which will give a (large) boundary value problem of ODEs. To solve the latter, we will use a multiple shooting method, whereby the interval $[0, 1]$ is partitioned into several subintervals, $[0, 1] = \cup_{i=0}^{K-1}[t_i, t_{i+1}]$, initial guesses for the density and the velocity are provided at each t_i, $i = 0, \ldots, K-1$, initial value problems are solved

on $[t_i, t_{i+1}]$, and eventually enforcement of continuity and boundary conditions will result in a large nonlinear system to solve for the density ρ and velocity v at each t_i. To solve the nonlinear system, we use Newton's method, and—to enhance its convergence properties—we will adopt a continuation method to obtain good initial guesses for the Newton's iteration.

Multiple shooting is a well-studied technique for solving two-point boundary value problems of ordinary differential equations (TPBVPs of ODEs), and we refer the reader to [19] for an early derivation of the method, and to [1] for a comprehensive review of techniques for solving TPBVPs of ODEs, and relations (equivalence) between many of them. Our main reason for adopting multiple shooting is its overall simplicity, and the ease with which we can adopt appropriate time discretizations of symplectic type (on sufficiently short time intervals) in order to avoid finite time singularities when solving (1.2) subject to given initial conditions. We would like to remark that the convergence analysis of the multiple shooting method, together with the space-time discretization and continuous method, is beyond the scope of the current paper and will be studied in the future. With regard to the spatial discretization of Wasserstein Hamiltonian flow, the convergence result of the Fisher information regularization symplectic scheme has been obtained in [10].

The rest of this paper is organized as follows. In section 2, we briefly review the continuous OT problem and introduce a spatial discretization to convert (1.2) into Hamiltonian ODEs. First, we propose the semidiscretization for the (ρ, S) variables, but then in section 3 we will revert it to the (ρ, v) variables, which are those with which we end up working. The multiple shooting method, and the continuation strategy, are also presented in section 3. Results of numerical experiments are presented in section 4.

2. Spatially discrete OT problems. In this section, we introduce the spatial discretization of (1.2). First, we need to truncate $\mathbb{R}^d$ to a finite computational domain, which for us will be a d-dimensional rectangular box in $\mathbb{R}^d$: $\mathcal{O} = [x_L, x_R]^d$. We note that truncating $\mathbb{R}^d$ to a domain like $\mathcal{O}$ is effectively placing some natural condition on the type of densities μ and ν we envision having, namely they need to decay sufficiently fast outside of the box $\mathcal{O}$ (see [16]). Then, we propose the spatial discretization of (1.2) by following the theory of the OT problem on a finite graph similarly to what we did in [10].

Next, we let $G = (V, E)$ be a uniform lattice graph with equal spatial step-size $\delta x = \frac{x_R - x_L}{n}$ in each dimension. Here V is the vertex set with $N = (n+1)^d$ nodes labeled by multi-index $i = (i_k)_{k=1}^d \in V, i_k \leq n+1$. E is the edge set: $ij \in E$ if $j \in N(i)$ (read, j is a neighbor of i), where

$$N(i) = \cup_{k=1}^d N_k(i), \quad N_k(i) = \Big\{(i_1, \ldots, i_{k-1}, j_k, i_{k+1}, \ldots, i_d) \big| |i_k - j_k| = 1\Big\}.$$

A vector field v on E is a skew-symmetric matrix. The inner product of two vector fields u, v is defined by

$$\langle u, v\rangle_{\theta(\rho)} := \frac{1}{2} \sum_{(j,l)\in E} u_{jl} v_{jl} \theta_{jl}(\rho),$$

where θ is a weight function depending on the probability density. In this study, we select it as the average of density on neighboring points, i.e.,

$$\theta_{ij}(\rho) := \frac{\rho_i + \rho_j}{2} \quad \text{if} \quad j \in N(i). \tag{2.1}$$

For more choices, we refer the reader to [10] and references therein.

The discrete divergence of the flux function ρv is defined as

$$div_G^\theta(\rho v) := -\Big(\sum_{l\in N(j)} \frac{1}{\delta x} v_{jl}\theta_{jl}\Big)_{j=1}^N.$$

Using the discrete divergence and inner product, a discrete version of the Benamou–Brenier formula is introduced in [7],

$$W^2(\mu,\nu) = \inf_{\widetilde{v}} \Big\{ \int_0^1 \langle \widetilde{v}, \widetilde{v}\rangle_{\theta(\rho)} dt \ : \ \frac{d\rho}{dt} + div_G^\theta(\rho\widetilde{v}) = 0,\ \rho(0)=\mu,\ \rho(1)=\nu \Big\}. \tag{2.2}$$

Considering the critical point (ρ, v, λ) of the Lagrange multiplier of (2.2),

$$\int_0^1 \langle \widetilde{v}, \widetilde{v}\rangle_{\theta(\rho)} dt + \int_0^1 \sum_{i=1}^N \lambda_i \Big(\frac{d\rho_i}{dt} + div_G^\theta(\rho\widetilde{v})|_i\Big) dt,$$

we have that

$$\begin{aligned} &\Big(2\widetilde{v}_{ij} + \frac{\lambda_j - \lambda_i}{\delta x}\Big)\theta_{ij}(\rho) = 0, \\ &\sum_{j\in N(i)} |\widetilde{v}_{ij}|^2 - \frac{d\lambda_i}{dt} - \sum_{j\in N(i)} \frac{\lambda_i - \lambda_j}{\delta x}\widetilde{v}_{ij} = 0. \end{aligned}$$

When $\theta_{ij}(\rho) > 0, ij \in E$, we have $\widetilde{v}_{ij} = \frac{\lambda_i - \lambda_j}{2\delta x}$, which leads to the gradient structure of $\widetilde{v}_{ij}$. By letting $\widetilde{v}_{ij} = \frac{S_i - S_j}{\delta x}$ for $ij \in E$, its critical point satisfies the discrete Wasserstein Hamiltonian flow (cf. (1.2)),

$$\begin{aligned} &\frac{d\rho_i}{dt} = \sum_{j\in N(i)} \frac{1}{(\delta x)^2}(S_i - S_j)\theta_{ij}(\rho) = \frac{\partial \mathcal{H}}{\partial S_i}, \\ &\frac{dS_i}{dt} = -\frac{1}{2}\sum_{j\in N(i)} \frac{1}{(\delta x)^2}(S_i - S_j)^2 \frac{\partial \theta_{ij}(\rho)}{\partial \rho_i} = -\frac{\partial \mathcal{H}}{\partial \rho_i} + C(t) \end{aligned} \tag{2.3}$$

with boundary values $\rho(0) = \mu$ and $\rho(1) = \nu$. Here the discrete Hamiltonian is

$$\mathcal{H}(\rho, S) = \frac{1}{4}\sum_{i=1}^N \sum_{j\in N(i)} \frac{|S_i - S_j|^2}{(\delta x)^2}\theta_{ij}(\rho).$$

We observe that (2.3) is a semidiscrete version of the Wasserstein Hamiltonian flow, preserving the Hamiltonian and symplectic structure of the original system (1.2). Likewise, the Wasserstein distance $W(\mu,\nu)$ can be approximated by $\sqrt{2\mathcal{H}(\mu, S^0)}$, where S^0 is the initial condition of the spatially discrete S. Finally, define the density set by

$$\mathcal{P}(G) = \Big\{ \rho = (\rho_i)_{i\in V} \Big| \sum_{i\in V} \rho_i (\delta x)^d = 1, \rho_i \geq 0, i \in V \Big\},$$

where ρ_i represents the density on node i. The interior of $\mathcal{P}(G)$ is denoted by $\mathcal{P}_o(G)$.

In this study, (2.3) is the underlying spatial discretization for our numerical method (see (3.2) below), in large part because of the following result which gives some important properties of (2.3), and whose proof is in [10, Proposition 2.1].

PROPOSITION 2.1. *Consider* (2.3) *with initial values* μ *and* S^0*, and let* T^* *be the first time the system develops a singularity. Then, for any* $\mu \in \mathcal{P}_o(G)$ *and any function* S^0 *on* V*, there exists a unique solution of* (2.3) *for all* $t < T^*$*, and it satisfies the following properties for all* $t < T^*$*.*

(i) *Mass is conserved:*

$$\sum_{i=1}^{N} \rho_i(t) = \sum_{i=1}^{N} \mu_i^0.$$

(ii) *Energy is conserved:*

$$\mathcal{H}(\rho(t), S(t)) = \mathcal{H}(\mu, S^0).$$

(iii) *Symplectic structure is preserved:*

$$d\rho(t) \wedge dS(t) = d\mu \wedge dS^0,$$

i.e., the sum of oriented areas of projections onto the coordinate planes (ρ_1, S_1), $\ldots$, (ρ_N, S_N) *is an integral invariant, where* $\wedge$ *is the exterior product of two differential forms.*

(iv) *The solution is time reversible: if* $(\rho(t), S(t))$ *is the solution of* (2.3)*, then* $(\rho(-t), -S(-t))$ *also solves it.*

(v) *Time invariants* $\widetilde{\rho} \in \mathcal{P}_o(G)$ *and* $\widetilde{S}(t) = -vt$ *form an interior stationary solution of* (2.3) *if and only if* $\mathcal{H}(\rho, S)$ *is spatially independent (we denote it as* $\mathcal{H}(\rho)$ *in this case) and* $\widetilde{\rho}$ *is the critical point of* $\min_{\rho \in \mathcal{P}_o(G)} \mathcal{H}(\rho)$ *and* $v = \mathcal{H}(\widetilde{\rho})$*.*

The above discretization is motivated by the formulation presented in [8], where the goal is to study OT on discrete structures, such as a graph. We use it as our spatial discretization scheme. Hence, it inherits many properties of the original problem. For more pros/cons of this choice, we refer the reader to [10] and references therein.

3. Algorithm. In this section, we first present the ideas of shooting methods, then combine them with a continuation strategy to design our algorithm for approximating the solution of the OT problem (1.1).

3.1. Single shooting. To illustrate the single shooting strategy, consider (2.3) in the time interval $[0, 1]$. Assuming that it exists, denote with $\rho(t, S^0)$, $t \in [0, 1]$, the solution of (2.3) with initial values (μ, S^0). To satisfy the boundary value at $t = 1$, one needs to find S^0 such that the trajectory starting at (μ, S^0) passes through ν at $t = 1$, i.e.,

$$\rho(1, S^0) - \nu = 0. \tag{3.1}$$

To solve (3.1), root-finding algorithms must be used to update the current guess of S^0 to achieve better approximations. For example, when using Newton's method, the updates are supposedly computed by

$$J(1, S^{(i)}) \left(S^{(i+1)} - S^{(i)} \right) = -(\rho(1, S^{(i)}) - \nu), \quad i = 0, 1, \ldots,$$

where $J(t, S) = \frac{\partial \rho(t,S)}{\partial S}$ is the Jacobian of $\rho(t, S) - \nu$ with respect to S. To ensure successful computations in Newton's method, finding a good initial guess for S^0 and having an invertible Jacobi matrix are crucial. But, as we anticipated in Remark 1.1, the Jacobian matrix $J(t, S)$ is singular, as otherwise a solution of (3.1) ought to

be isolated, which can't be true, since adding an arbitrary constant will still give a solution.

To remedy this situation, we revert to the (ρ, v) formulation and rewrite the Hamiltonian system (2.3) into an equivalent form in terms of (ρ, v). More precisely, letting $v_{ij} = S_i - S_j$, (2.3) becomes

$$\begin{aligned} \frac{d\rho_i}{dt} &= -\sum_{j\in N(i)} \frac{1}{(\delta x)^2} v_{ij}\theta_{ij}(\rho), \\ \frac{dv_{ij}}{dt} &= \frac{1}{2}\sum_{k\in N(j)} \frac{1}{(\delta x)^2} v_{kj}^2 \frac{\partial \theta_{jk}(\rho)}{\partial \rho_j} - \frac{1}{2}\sum_{k\in N(i)} \frac{1}{(\delta x)^2} v_{ki}^2 \frac{\partial \theta_{ik}(\rho)}{\partial \rho_i}. \end{aligned} \tag{3.2}$$

Since v_{ij} is the difference between S_j and S_i, a constant shift in S has no impact on the values of $v = \{v_{ij}\}$. On the other hand, there are now many redundant equations in (3.2), because $\{v_{ij}\}$ are not independent variables. For example, they must satisfy $v_{ij} = -v_{ji}$. Furthermore, there are a total of $N = (n+1)^d$ unknown values for S, while there are $2dn(n+1)^{d-1}$ unknowns for v on the lattice graph G. Clearly, to determine S up to a constant, only $N-1$ values for v are needed. In other words, there must be only $N-1$ independent v-equations in (3.2) to be solved, and the remaining ones are redundant and must be removed so that the resulting system leads to a nonsingular Jacobian.

There are different ways to remove the redundancies. To illustrate this in a simple setting, let us consider the 1-dimensional case ($d = 1$), in which the lattice graph G has $n-1$ interior nodes and 2 boundary nodes. Each interior node has two neighbors while a boundary node has only one neighbor. We have at least two options: either keep all equations for $v_{i,i+1}$, $i = 1, \ldots, (N-1)$, or keep the equations for $v_{i,i-1}$, $i = 2, \ldots, N$. Adopting the first choice, we have the following equations to solve:

$$\begin{aligned} \frac{d\rho_i}{dt} &= \frac{1}{(\delta x)^2} v_{(i-1)i}\theta_{(i-1)i}(\rho) - \frac{1}{(\delta x)^2} v_{i(i+1)}\theta_{i(i+1)}(\rho), \\ \frac{dv_{i(i+1)}}{dt} &= \frac{1}{4}\frac{1}{(\delta x)^2} v_{(i-1)i}^2 - \frac{1}{4}\frac{1}{(\delta x)^2} v_{i(i+1)}^2 \end{aligned} \tag{3.3}$$

for all $i = 1, \ldots, N-1$. If we take no-flux boundary conditions for (ρ, v), we have $v_{01} = 0, \theta_{01} = 0$. Finally, mass conservation gives the condition $\rho_N = \frac{1-\delta x \sum_{i=1}^{N-1} \rho_i}{\delta x}$.

Denoting $v(0) = v^0 = \{v^0_{i,i+1}\}_{i=1}^{N-1} = \{S^0_{i+1} - S^0_i\}_{i=1}^{N-1}$, and the solution of (3.3) with initial values (μ, v^0) as $\rho_t = \rho(t, v^0)$, $v_t = v(t, v^0)$, we can revise the single shooting strategy in terms of (ρ, v) as finding the initial velocity v^0 such that $\rho(1, v^0) = \nu$. By applying Newton's method, we obtain

$$\hat{J}(1, v^{(m)})\big(v^{(m+1)} - v^{(m)}\big) = -(\rho(1, v^{(m)}) - \nu), \quad m = 0, 1, \ldots,$$

where $\hat{J}(1, v^{(m)}) = \left[\frac{\partial \rho_t}{\partial v^0}\right]_{1, v^{(m)}}$ is the Jacobian of $\rho(t, v(0)) - \nu$ with respect to $v(0)$, evaluated at $t = 1$, $v = v^{(m)}$. For later reference, and since ν plays no role in the definition of $\hat{J}$, let us define the function

$$\hat{J}(t, v^0) = \left[\frac{\partial \rho}{\partial v^0}\right]_{t,v}, \quad t \geq 0\ .$$

Now, the single shooting strategy we just outlined is plagued by a common shortfall of single shooting techniques, namely that the initial guess $v^{(0)}$ must be quite

close to the exact solution. In the present context, this is further exacerbated by the fact that (1.2) may develop singularities in finite time (see, e.g., [10]), and as a consequence the choice of a poor initial guess may (and does) lead to finite time blow-up of the solution of the initial value problem. To overcome this serious difficulty, we now give a result showing that the function $\hat{J}(t, v^0)$ remains invertible for sufficiently short times, and later will exploit this result to justify adopting a multiple shooting strategy.

LEMMA 3.1. *Let G be a 1-dimensional uniform lattice graph, and let $t_1 > 0$ be sufficiently small. Assume that (ρ, v) is the smooth solution of (3.3) satisfying $\mu > 0$. Then, the function $\hat{J}(t, v^0)$ is invertible for $t \in (0, t_1]$.*

Proof. Direct calculation shows that the function $\hat{J}(t, v^0) = \frac{\partial}{\partial v^0}\rho(t, v^0)$ satisfies

$$\frac{d}{dt}\frac{\partial \rho_t}{\partial v^0} = B_{11}\frac{\partial v_t}{\partial v^0} + B_{12}\frac{\partial \rho_t}{\partial v^0}, \quad \hat{J}(0, v^0) = 0_{n\times n},$$
$$\frac{d}{dt}\frac{\partial v_t}{\partial v^0} = B_{22}\frac{\partial v_t}{\partial v^0}, \quad \left[\frac{\partial v_t}{\partial v^0}\right]_{t=0} = I,$$

where

$$(B_{11})_{ii} = -\frac{\rho_i + \rho_{i+1}}{2(\delta x)^2}, \quad i = 1, \dots, n-1,$$
$$(B_{11})_{i,i-1} = \frac{\rho_i + \rho_{i-1}}{2(\delta x)^2}, \quad i = 2, \dots, n,$$
$$(B_{11})_{nn} = \frac{1 - \sum_{i=1}^{n-1}\rho_i \delta x}{2(\delta x)^3},$$
$$(B_{12})_{11} = -\frac{v_1}{2(\delta x)^2}, (B_{12})_{ii}(\rho, v) = -\frac{v_i}{2(\delta x)^2} + \frac{v_{i-1}}{2(\delta x)^2}, \quad i = 2, \dots, n,$$
$$(B_{12})_{i,i-1} = \frac{v_{i-1}}{2(\delta x)^2}, (B_{12})_{i,i+1} = -\frac{v_i}{2(\delta x)^2}, \quad i = 2, \dots, n-1,$$
$$(B_{12})_{n,i} = \frac{v_n}{2(\delta x)^2}, \quad i = 1, \dots, n-2, \quad (B_{12})_{n,n-1} = \frac{v_n}{2(\delta x)^2} + \frac{v_{n-1}}{2(\delta x)^2},$$
$$(B_{22})_{i,i+1} = -\frac{1}{2(\delta x)^2}v_{i+1}, \ i = 1, \dots, n-1, \quad (B_{22})_{i,i-1} = \frac{1}{2(\delta x)^2}v_{i-1}, \ i = 2, \dots, n.$$

Since B_{11} is a lower triangular matrix, it is invertible if and only if

$$\min_{i\le n}(\theta_{i,i+1}(\rho)) > 0,$$

where θ_{ij} is defined in (2.1) and hence $\theta_{i,i+1}(\rho) > 0$ for as long as ρ remains positive. Moreover, given the initial condition to the identity for $\frac{\partial v_t}{\partial v^0}$, if $t_1 > 0$ is sufficiently small, the matrix $\frac{\partial v_t}{\partial v^0}$ remains invertible. Furthermore, since $\hat{J}(0, v^0) = 0_{n\times n}$, we conclude that for $t > 0$ sufficiently small,

$$\hat{J}(t, v^0) \approx tB_{11} + \mathcal{O}(t^2),$$

which implies that $\hat{J}(t, v^0)$ is invertible for $t > 0$, and sufficiently small. ∎

Once v values become available, if desired we can reconstruct S on the lattice graph G from the relation $v_{ij} = S_i - S_j$.

We conclude this section by emphasizing that the semidiscretization (3.2) is a spatial discretization of the Wasserstein geodesic equations written in terms of (ρ, v) [10].

However, this semidiscretization has been arrived at by designing a semidiscretization scheme for the system (1.2) in the (ρ, S) variables, respecting the Hamiltonian nature of the problem; see (2.3) and Proposition 2.1.

3.2. Multiple shooting method. As proved in Lemma 3.1, in the 1-dimensional case the function $\hat{J}(t, v^0)$ is invertible for sufficiently short times; however, for the success of single shooting, this ought to be invertible at $t = 1$, a fact which is often violated. In addition, our numerical experiments indicate poor stability behavior when using the single shooting method to solve the Wasserstein geodesic equations (2.3). To mitigate these drawbacks, we propose using multiple shooting.

We partition the interval $[0, 1]$ into the union of subintervals $[t_k, t_{k+1}], k = 0, \ldots, K-1$, and let $\delta t = \max_k(t_{k+1} - t_k)$. For example, we could take $t_k = k\delta t$ and $K\delta t = 1$. To illustrate, we again take G as the d-dimensional uniform lattice graph. In each subinterval $[t_k, t_{k+1}], k = 0, \ldots, K-1$, (2.3) is converted into equations in terms of (ρ, v), just like the ones in (3.2),

$$\frac{d\rho_i^{k+1}}{dt} = -\sum_{j\in N(i)} \frac{1}{(\delta x)^2} v_{ij}^{k+1}\theta_{ij}(\rho),$$
$$\frac{dv_{ij}^{k+1}}{dt} = \frac{1}{2}\sum_{l\in N(j)} \frac{1}{(\delta x)^2}(v_{jl}^{k+1})^2 \frac{\partial\theta_{lj}(\rho)}{\partial\rho_j} - \frac{1}{2}\sum_{m\in N(i)} \frac{1}{(\delta x)^2}(v_{mi}^{k+1})^2 \frac{\partial\theta_{ik}(\rho)}{\partial\rho_i},$$

where $i \in N$ is a multi-index for a grid point in d-dimensional lattice. The superscript $k+1$ in ρ and v indicates that the corresponding variables are defined in the subinterval $[t_k, t_{k+1}]$. Then, the multiple shooting method requires finding the values of ρ, v at temporal points $\{t_k\}_{k=0}^{K-1}$, i.e.,

$$(\widetilde{v}^0, \widetilde{\rho}^1, \widetilde{v}^1, \ldots, \widetilde{\rho}^{K-1}, \widetilde{v}^{K-1})^T,$$

such that the continuity conditions hold; that is, for $k = 0, \ldots, K-2$,

$$F_{2k+1}(\widetilde{\rho}^k, \widetilde{v}^k, \widetilde{\rho}^{k+1}) = \rho^{k+1}(t_{k+1}, \widetilde{\rho}^k, \widetilde{v}^k) - \widetilde{\rho}^{k+1} = 0,$$
$$F_{2k+2}(\widetilde{\rho}^k, \widetilde{v}^k, \widetilde{v}^{k+1}) = v^{k+1}(t_{k+1}, \widetilde{\rho}^k, \widetilde{v}^k) - \widetilde{v}^{k+1} = 0.$$

When $k = 0$ and $k = K-1$, the given boundary values $\rho(0) = \mu$ and $\rho(1) = \nu$ yield that

$$F_1(\mu, \widetilde{v}^0, \widetilde{\rho}^1) = \rho^1(t_1, \mu, \widetilde{v}^0) - \widetilde{\rho}^1 = 0,$$
$$F_{2K-1}(\widetilde{\rho}^{K-1}, \widetilde{v}^{K-1}, \nu) = \rho^K(t_K, \widetilde{\rho}^{K-1}, \widetilde{v}^{K-1}) - \nu = 0.$$

As is customary, we use Newton's method to find the root $(\widetilde{v}^0, \widetilde{\rho}^1, \widetilde{v}^1, \ldots, \widetilde{\rho}^{K-1}, \widetilde{v}^{K-1})$ of $F = (F_w)_{w=1}^{2K-1} = 0$. To this end, we first need to remove the redundant equations for the velocity field v. The number of unknown variables in ρ is $N-1 = (n+1)^d - 1$, which is one fewer than the total number of nodes in G, because the total probability must be one. The number of unknowns in S is N. The vector field v contains the differences in S, hence the total number of independent variables in v is also $N-1$, due to the connectivity of G. The following lemma ensures that we can always find the $N-1$ components of v from which one can generate all the components of v on the lattice graph G.

LEMMA 3.2. *Given a connected d-dimensional lattice graph G and a vector field v which is generated by a potential S on G, there exists a subset consisting of $N-1$*

components of v, denoted by $\widehat{v} = (\widehat{v}_w)_{w=1}^{N-1}$, such that any v_{ij} can be expressed as a combination of the entries of $\widehat{v}$, i.e.,

$$v_{ij} = \sum_{w=1}^{N-1} a_w \widehat{v}_w, \quad \textit{where} \quad a_w = 1, \ \textit{or} \ -1, \ \textit{or} \ 0\ . \tag{3.4}$$

Proof. Since G is connected, there is always a path on the graph passing through all the nodes of G and with exactly $N-1$ edges. For convenience, we denote $\widehat{v}_w = \widehat{v}_{i_w i_{w+1}}$, the value of v on the edge $i_w i_{w+1}$ along the path. According to the assumption that v is generated by a potential S, i.e., $v_{ij} = S_i - S_j$, we have that $\widehat{v}_w = S_{i_w} - S_{i_{w+1}}$. Since $\{i_w\}_{w \le N-1}$ is a permutation of the node set V, we could use $S_{i_w} - S_{i_{w+1}}, w \le N-1$ to reconstruct other $v_{ij}, ij \in E$ by the connectivity of G. For example, we may assume that $i = i_{w_1}, j = i_{w_L}$ for some w_1, w_L, $L \le N$ such that $i_{w_1} i_{w_2}, \ldots, i_{w_{L-1}} i_{w_L}$ belongs to the path passing through all the nodes; then $v_{ij} = S_{i_{w_1}} - S_{i_{w_L}} = \sum_{l=1}^{L-1} S_{i_{w_l}} - S_{i_{w_{l+1}}} = \sum_{l=1}^{L-1} \widehat{v}_{w_l}$. Therefore, all entries of v can be expressed as the above combination of the entries $(\widehat{v}_w)_{w=1}^{N-1}$. ∎

Remark 3.1. By using (3.3) and (3.5) for 1-dimensional and 2-dimensional problems, we have effectively made a specific choice of $\widehat{v}$ in Lemma 3.2. For instance, the choice of $\widehat{v}$ in two dimensions is shown in Figure 3.1. Of course, other choices are possible.

From the proof, we observe that the choice of $\widehat{v}$ is not unique, since every path going through all nodes of G using $N-1$ edges will give a system with no redundancy. The edges could be passed multiple times. Let us select one such choice and denote it by $(\widehat{v}_w)_{w=1}^{N-1}$. For instance, in 2-dimensional lattice graph G, we choose the $\widehat{v}$ that generates the vector field (see Figure 3.1) as follows. Denote every node on G by $(i,j)_{i,j=1}^{n+1}$. For fixed i, $(i,j)_{j=1}^{n+1}$ becomes a 1-dimensional lattice graph in the x_2 direction. Following (3.3), we choose $\widehat{v}_w = v_{(i,j)(i,j+1)}$ for $w = n \times (i-1) + j$, $j = 1, \ldots, n, i = 1, \ldots, n+1$, which gives $(n+1) \times n$ components of $\widehat{v}_w$. Because of the connectivity of G relative to the x_1 direction, the last n components of $\widehat{v}_w$ are chosen by $\widehat{v}_w = v_{(j,1)(j+1,1)}$ for $w = (n+1) \times n + j$, $j = 1, \ldots, n$. For convenience, let us denote the velocity on the related edges in this path by $\{v_{i_w i_{w+1}}\}_{w=1}^{N-1} = \{\widehat{v}_w\}_{w=1}^{N-1}$. Then the reduced Wasserstein system (2.3) becomes

$$\begin{aligned}
\frac{d\rho_{i_w}^{k+1}}{dt} &= \sum_{j \in N(i_w)} v_{j i_w}^{k+1} \theta_{i_w j}(\rho), \\
\frac{dv_{i_w}^{k+1}}{dt} &= \frac{1}{2} \sum_{j \in N(i_w)} \frac{1}{(\delta x)^2} (v_{i_w,j}^{k+1})^2 \frac{\partial \theta_{i_w j}(\rho)}{\partial \rho_{i_w}} \\
&\quad - \frac{1}{2} \sum_{m \in N(i_{w+1})} \frac{1}{(\delta x)^2} (v_{i_{w+1},m}^{k+1})^2 \frac{\partial \theta_{i_{w+1} j}(\rho)}{\partial \rho_{i_{w+1}}},
\end{aligned} \tag{3.5}$$

where v_{ij} satisfies (3.4) and the unknowns are $(\rho, \widehat{v})$ with

$$\begin{aligned}
&\rho^{k+1}(t_k, \rho(t_k), \widehat{v}(t_k)) = \rho(t_k), \quad \rho^{k+1}(t_{k+1}, \rho(t_k), \widehat{v}(t_k)) = \rho(t_{k+1}), \\
&\widehat{v}^{k+1}(t_k, \rho(t_k), \widehat{v}(t_k)) = \widehat{v}(t_k), \quad \widehat{v}^{k+1}(t_{k+1}, \rho(t_k), \widehat{v}(t_k)) = \widehat{v}(t_{k+1}).
\end{aligned}$$

We apply the multiple shooting method to (3.5), i.e., we look for the root $Z =$

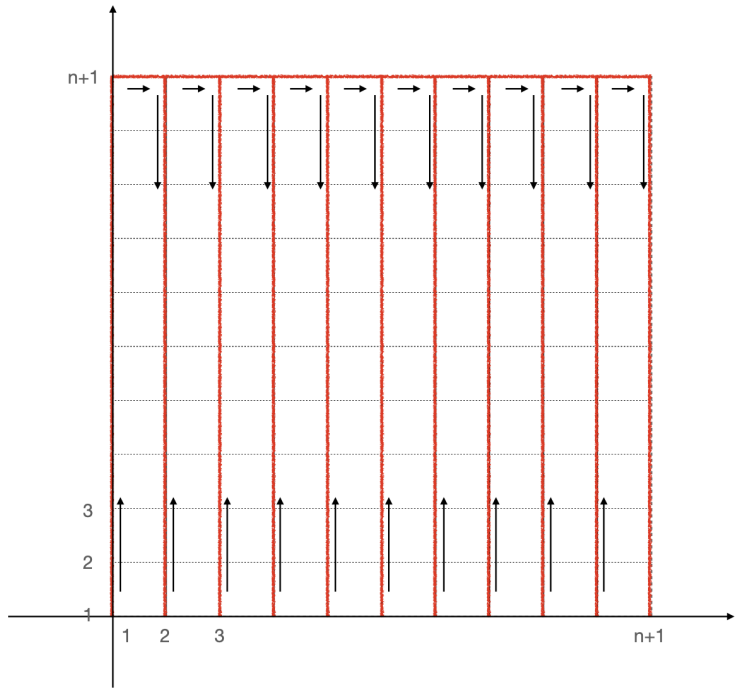

FIG. 3.1. *The edges (in red) of $\hat{v}$ that generate the velocity in the 2-dimensional lattice graph. The path is indicated by the arrows. Clearly, many edges are passed twice. (Figure in color online.)*

$(\widehat{v}^0, \rho^1, \widehat{v}^1, \ldots, \rho^{K-1}, \widehat{v}^{K-1})$ of F defined by

$$
\begin{aligned}
F_{2k+1}(\rho^k, \widehat{v}^k, \rho^{k+1}) &= \rho^{k+1}(t_{k+1}, \rho^k, \widehat{v}^k) - \rho^{k+1} = 0, \\
F_{2k+2}(\rho^k, \widehat{v}^k, \widehat{v}^{k+1}) &= \widehat{v}^{k+1}(t_{k+1}, \rho^k, \widehat{v}^k) - \widehat{v}^{k+1} = 0, \ k \le K-2, \\
F_{2K-1}(\rho^{K-1}, \widehat{v}^{K-1}, \rho^K) &= \rho^K(t_{K-1}, \rho^{K-1}, \widehat{v}^{K-1}) - \nu = 0,
\end{aligned}
\tag{3.6}
$$

where $\rho^0 = \mu, \rho^K = \nu$.

The use of Newton's method to solve (3.6) gives

$$
A^{(m)} \Delta Z^{(m)} = -F^{(m)}, \tag{3.7}
$$

where m is the iteration index, $\Delta Z^{(m)} = Z^{(m+1)} - Z^{(m)}$,

$$
Z^{(m)} = (v^{0,(m)}, \rho^{1,(m)}, v^{1,(m)}, \ldots, v^{K-1,(m)}, \rho^{K-1,(m)})^T,
$$

$F^{(m)} = (F_1(Z^{(m)}), F_2(Z^{(m)}), \ldots, F_{2K-1}(Z^{(m)}))^T$, and $A^{(m)}$ is the Jacobian of F, whose structure is as follows, where the X correspond to nonzero $(N-1) \times (N-1)$

matrices:

$$\begin{pmatrix} X & X & 0 & 0 & 0 & & & & & \\ X & 0 & X & 0 & 0 & & & & & \\ 0 & X & X & X & 0 & & & & & \\ 0 & X & X & 0 & X & & & & & \\ & & & X & X & X & 0 & & & \\ & & & X & X & 0 & X & & & \\ & & & & & & & \ddots & \ddots & \\ & & & & & & X & X & X & 0 \\ & & & & & & X & X & 0 & X \\ & & & & & & & & X & X \end{pmatrix}.$$

Omitting the superscript m in the expressions of $A^{(m)}$, the blocks $A_{ij}, i, j = 1, \ldots, 2K-1$ are easily seen to be the following. For $i = 2, \ldots, K-1$,

$$A_{2(i-1)+1,2(i-1)} = \frac{\partial \rho^i(t_i, v^{i-1}, \rho^{i-1})}{\partial v^{i-1}}, \quad A_{2(i-1)+1,2(i-1)+1} = \frac{\partial \rho^i(t_i, v^{i-1}, \rho^{i-1})}{\partial \rho^{i-1}},$$

$$A_{2i,2(i-1)} = \frac{\partial v^i(t_i, v^{i-1}, \rho^{i-1})}{\partial v^{i-1}}, \quad A_{2i,2(i-1)+1} = \frac{\partial v^i(t_i, \rho^{i-1}, \rho^{i-1})}{\partial \rho^{i-1}},$$

$$A_{2(i-1)+1,2i} = -I, \quad A_{2i,2i+1} = -I,$$

$$A_{11} = \frac{\partial \rho^1(t_1, v^0)}{\partial v^0}, \quad A_{12} = -I,$$

$$A_{21} = \frac{\partial v^1(t_1, v^0)}{\partial v^0}, \quad A_{23} = -I,$$

and

$$A_{2K-1,2K-2} = \frac{\partial \rho^K(t_K, v^{K-1}, \rho^{K-1})}{\partial v^{K-1}}, \quad A_{2K-1,2K-1} = \frac{\partial \rho^K(t_K, v^{K-1}, \rho^{K-1})}{\partial \rho^{K-1}}.$$

Below, we show invertibility of $A^{(m)}$ for δt sufficiently small.

THEOREM 3.1. *Let (ρ, v) be the unique solution of (3.2), and let $Z^* = (v(0), \rho(t_1), v(t_1), \ldots, \rho(t_{K-1}), v(t_{K-1}))^T$ be the exact solution evaluated at the multiple shooting points. Assume that the initial vector $Z^{(0)}$ is sufficiently close to Z^*, i.e., $|Z^{((0)} - Z^*| = \mathcal{O}(\epsilon)$ for $\epsilon > 0$ sufficiently small, (ρ, v) is continuously differentiable in $[0,1]$ satisfying $(\rho, v) \in \mathcal{C}_b^2([0,1]; \mathbb{R}^N) \times \mathcal{C}_b^2([0,1]; \mathbb{R}^N \times \mathbb{R}^N)$ and $\min_{t\in[0,T]} \min_{i=1}^N \rho_i \geq c > 0$, and that $\frac{\partial \rho(1, \rho^0, v^0)}{\partial v^0}$ is invertible. Then, Newton's method of the multiple shooting method (3.7) is quadratically convergent to Z^* for δt sufficiently small.*

Proof. By standard Newton's convergence theory, it will be enough to prove the invertibility of Jacobian matrix $A^{(0)}$ for appropriately small ϵ and δt. Rewrite $A^{(0)}$ in partitioned form $\begin{pmatrix} A'_{11} & A'_{12} \\ O_{N-1,N-1} & A'_{22} \end{pmatrix}$, where A'_{11} is a $(2K-2)n \times n$ matrix, A'_{12} is a $(2K-2)n \times (2K-2)n$ matrix, and A'_{22} is a $(N-1) \times (2K-2)(N-1)$ matrix. Using the property of determinant for the partitioned matrix and the fact that $\det(A'_{12}) = 1$, and writing A in lieu of $A^{(0)}$, we have

$$\begin{aligned} \det(A) &= \det \begin{pmatrix} 0_{N-1 \times N-1} & A'_{22} \\ A'_{11} & A'_{12} \end{pmatrix} \\ &= \det(A'_{12}) \det(0_{N-1 \times N-1} - A'_{22}(A'_{12})^{-1} A'_{11}) \\ &= (-1)^{N-1} \det(A'_{22}(A'_{12})^{-1} A'_{11}). \end{aligned}$$

So, we are left to show that $\det(A'_{22}(A'_{12})^{-1}A'_{11}) \neq 0$. The structure of A'_{12} implies that

$$A'_{22}(A'_{12})^{-1}A'_{11} = \left(\frac{\partial \rho^{K,(0)}}{\partial \rho^{K-1,(0)}}, \frac{\partial \rho^{K,(0)}}{\partial v^{K-1,(0)}}\right) \prod_{i=2}^{K-1} \begin{pmatrix} \frac{\partial \rho^{i,(0)}}{\partial \rho^{i-1,(0)}} & \frac{\partial \rho^{i,(0)}}{\partial v^{i-1,(0)}} \\ \frac{\partial v^{i,(0)}}{\partial \rho^{i-1,(0)}} & \frac{\partial v^{i,(0)}}{\partial v^{i-1,(0)}} \end{pmatrix} \left(\frac{\partial \rho^{1,(0)}}{\partial v^{0,(0)}}, \frac{\partial v^{1,(0)}}{\partial v^{0,(0)}}\right)^T,$$

where $\rho^{i,(0)} = \rho^i(t_K, \rho^{i-1,(0)}, v^{i-1,(0)})$, $v^{i,(0)} = v^k(t_K, \rho^{i-1,(0)}, v^{i-1,(0)})$ for $i = 2, \ldots, K$, and $v^{1,(0)} = v^1(t_1, v^{0,(0)})$, $\rho^{1,(0)} = \rho^1(t_1, v^{0,(0)})$.

Now, invertibility of the Jacobian matrix A (or $A'_{22}(A'_{12})^{-1}A'_{11}$) follows from invertibility of the Jacobian matrix at the exact solution $\frac{\partial \rho(t_K, \rho^0, v^0)}{\partial v^0}$. To see this, due to (3.8), the continuous differentiability of the exact solution, and the assumption that $|Z^{(0,(m))} - Z^*| = \mathcal{O}(\epsilon)$, we have that

$$A'_{22}(A'_{12})^{-1}A'_{11} = \frac{\partial \rho(t_K, \rho^0, v^0)}{\partial v^0} + \mathcal{O}(\epsilon) + \mathcal{O}(\delta t).$$

Therefore, the invertibility of $\frac{\partial \rho(t_K, \rho^0, v^0)}{\partial v^0}$ with $t_K = 1$ implies the invertibility of the Jacobian matrix A. Combining with the assumption that ϵ and δ are sufficiently small, we obtain that $A^{(0)}$ is invertible in a neighborhood of Z^*, which, together with the boundedness assumption on ρ, v, implies the quadratic convergence of Newton's method. ∎

Remark 3.2. Of course, the initial value problems for the multiple shooting method must be integrated numerically. We have not accounted for this in Theorem 3.1. In principle, many choices are available to integrate these initial value problems, for instance, the symplectic integrators developed in [10] for Wasserstein Hamiltonian flows without regularization by Fisher information. In practice, when the subinterval number or the time step size is small enough, one could also use the classical Euler method to reduce the computational cost.

3.3. Continuation multiple shooting strategy. In light of Theorem 3.1, and notwithstanding the need for small δt, the multiple shooting method requires the initial guess to be near the exact solution Z^*. To make the method robust with respect to the initial guess, we adopt a standard continuation strategy by introducing a density function $f(\mu, \nu, \lambda)$, which is smooth with respect to a homotopy parameter $\lambda \in [0, 1]$ and satisfies

$$f(\mu, \nu, 0) = \mu, \quad f(\mu, \nu, 1) = \nu. \tag{3.8}$$

The specific choice of f in (3.8) depends on the initial and terminal distributions μ and ν. We illustrate below with two typical situations.

(a) "Gaussian-type" densities. If $\mu(x) = K_0 \exp(-c|x - b_0|^2)$ and $\nu(x) = K_1 \exp(-c|x - b_1|^2)$ with $\int_{\mathcal{O}} \mu dx = \int_{\mathcal{O}} \nu dx = 1$, we choose

$$f(\mu, \nu, \lambda)(x) = K_\lambda \exp(-c|x - b_0 - \lambda(b_1 - b_0)|^2)$$

with K_λ chosen so that $\int_{\mathcal{O}} f dx = 1$. For $\mu = K_0 \exp(-c_0|x - b_0|^2), \nu = K_1 \exp(-c_1|x - b_1|^2)$, we choose

$$f(\mu, \nu, \lambda)(x) = K_\lambda \exp(-(c_0 + \lambda(c_1 - c_0))|x - b_0 - \lambda(b_1 - b_0)|^2)$$

with K_λ chosen so that $\int_{\mathcal{O}} f dx = 1$.

(b) For general μ and ν, we choose f as the linear interpolant of μ and ν, which is automatically normalized. That is, we take

$$f(\mu, \nu, \lambda) = (1 - \lambda)\mu + \lambda\nu.$$

Remark 3.3. For our method to succeed, it is actually important that the densities be strictly positive (see Theorem 3.1). For this reason, and especially when the densities μ and ν are exponentially decaying (like Gaussians do), we add a small positive number, which we call *shift*, to the densities μ and ν and rescale them to keep the total probabilities equal to 1. In the numerical tests in section 4, these are the values r_0 and r_1 we use.

Using f, we consider the system (3.5) with λ dependent boundary conditions given by $\rho(0) = \mu$ and $\rho(1) = f(\mu, \nu, \lambda)$. Obviously, the problem with $\lambda_0 = 0$ is trivial to solve (the identity map), and it can be used as the initial guess for the solution at the value $\lambda_1 = \Delta\lambda$. By gradually increasing λ from 0 to 1, we eventually obtain the solution for (2.3) with boundary conditions μ and ν, which is the original Wasserstein geodesic problem we wanted to solve. This basic idea to use the solution with a smaller value of λ as the initial guess for the boundary value problem when the larger value of λ is well understood, and universal. In our context, it is important to note that this works because the OT problem always has an optimal map as long as μ and $f(\mu, \nu, \lambda)$ satisfy $\int_{\mathbb{R}^d} |x|^2 \mu dx, \int_{\mathbb{R}^d} |x|^2 f(\mu, \nu, \lambda) dx < +\infty$ (e.g., see [29]). In turn, this implies the existence of v or S (up to ρ_t-measure 0 sets) for the boundary value problem (BVP). In particular, this fact guarantees that a finite sequence $\{\lambda_j\}_{j \le L}$, $\lambda_L = 1$, and $Z^*_{\lambda_L}$ will be our approximation to the exact solution (ρ, v) at the multiple shooting points:

$$Z^0_{\lambda_0} := (v^{0,(0)}, \rho^{1,(0)}, \dots, v^{K-1,(0)}, \rho^{K-1,(0)})^{\mathcal{T}}. \tag{3.9}$$

For instance, we may take $v^{k,(0)}, k \le K - 1$, as constant vectors, $\rho^{k,(0)}, k \le K - 1$, from linear interpolation of $\rho^0 = \mu$ and $\rho^1 = f(\mu, \nu, \lambda_0)$, i.e.,

$$\rho^{k,(0)} = t_k \mu + (1 - t_k) f(\mu, \nu, \lambda_0), \quad k \le K - 1.$$

Finally, throughout all of our experiments, we enforced the following stopping criterion for the Newton iteration:

$$\frac{|F(Z^{(m+1)}) - F(Z^{(m)})|}{F(Z^{(m)})} < 10^{-5}. \tag{3.10}$$

We summarize the steps in the following algorithm.

Remark 3.4. Based on the output of Algorithm 3.1, the Wasserstein distance (or the Hamiltonian of (2.3)) can be easily obtained. From the first component $v^{0,*}$ of Z^*, we can reconstruct the initial values for S^0 as follows. The first component $v^{0,*} = (\widehat{v}_w)_{w=1}^{N-1}$, $\{i_w i_{w+1}\}_{w=1}^{N-1}$ generates the initial vector field. We first define the potential S on a fixed node i_0. Due to the connectivity of G, using $S_{i_{w+1}} = v_{i_w, i_{w+1}} + S_{i_w}$, we get the other initial values of S^0. Then the Wasserstein distance can be evaluated as $W(\mu, \nu) = \sqrt{2H(\mu, S^0)}$.

Remark 3.5 (barrier value for density). On rare occasions, we observed that during the Newton's iteration the updates became negative, leading to a failure. To avoid this phenomenon, we adopted a simple strategy, whereby we created a barrier for the values of the densities, and reset to this barrier any value which went below it. In our tests in section 4, use of this artificial barrier was needed only for Examples 4.8

Algorithm 3.1

Input: Multiple shooting points t_k, $k = 0, \ldots, K$, with $t_0 = 0$ and $t_K = 1$. Discrete densities μ, ν, on the spatial grid of size δx, continuation parameter λ, max-number of Newton's iterations `Maxits`.

Output: The minimizer Z^* at the multiple shooting points.

1: Follow (3.9) and produce a initial guess $Z^{(0)}_{\lambda_0}$;
2: Until $\lambda_j = 1$ or too many continuation steps, **do**
3: **for** $m = 1, 2, \ldots,$ `Maxits`, while (3.10) not satisfied **do**
4: Solve $J^{(m)}_{\lambda_j} d^{(m)} = -F(Z^{(m)}_{\lambda_j})$;
5: $Z^{(m+1)}_{\lambda_j} = Z^{(m)}_{\lambda_j} + d^{(m)}$;
6: **end for**
7: $\lambda_{j+1} = \lambda_j + \Delta\lambda$ (see Remark 3.6);
8: put $Z^0_{\lambda_{j+1}} = Z^*_{\lambda_j}$ as the new initial guess;
9: $j + 1 \to j$, go back to step 2.

and 4.12. To see this, in Example 4.8, we used the barrier at 10^{-5}, and in Example 4.12 the barrier was set at 10^{-3}. Clearly, with this strategy the total mass of the numerical solution is not exactly equal to 1, but the error incurred in the total mass is at the same level of the barrier value.

Remark 3.6 (choosing continuation steps). We implemented a very simple and conservative continuation strategy. In all of our tests, we first try to take $\lambda = 1$, to see whether this simple continuation is really needed. If the method does not work without continuation, we begin with a value λ_0 of λ for which multiple shooting works (e.g., we usually take $\lambda_0 = 0.1$ as the initial step), and choose a value $\Delta\lambda = \frac{1-\lambda_0}{L}$ with given L (e.g., $L = 10$ or 20 is our usual choice). We then try to continue by taking steps of size $\Delta\lambda$, though if the Newton's multiple shooting fails we decrease $\Delta\lambda$ by dividing the remaining interval by L again and/or increase the value of L by doubling it. In all tests of section 4, except Examples 4.1, 4.2, 4.4, and 4.6, the continuation strategy was used.

Remark 3.7 (choosing homotopy $f(\mu, \nu, \lambda)$). Finally, for all tests with Gaussian type densities μ, ν, we use the Gaussian interpolation (a) in subsection 3.3 for $f(\mu, \nu, \lambda)$. For other examples, we use the linear interpolation (b) in subsection 3.3 for $f(\mu, \nu, \lambda)$. To illustrate, in Example 4.8, we take $f(\mu, \nu, \lambda)$ as the normalization of $\exp(-5(x_2 - 0.5 - 1.95\lambda)^2 - 5(x_1 - 1.5 - 0.95\lambda)^2) + \exp(-5(x_2 - 0.5 - 1.95\lambda) - 5(x_1 - 1.5 + 0.95\lambda))^2 + r$ and obtain a sequence of λ's starting from $\lambda_0 = 0.1$, with $\Delta\lambda = 0.9/20$.

4. Numerical experiments. In this section, we apply Algorithm 3.1 to approximate the solution of several OT problems.[1] Throughout the experiments, the Jacobian in Newton's method is approximated by using a first order divided difference approximation of the derivatives. In the experiments, we observe that the majority of computational cost arose from assembling the Jacobian matrix. The spatial boundary conditions for the density functions are set to be homogeneous Neumann boundary conditions for all experiments except for Examples 4.1 and 4.2, which are subject to periodic boundary conditions. Except for this, Example 4.2, and Example 4.1, we do

[1]The MATLAB version of our code is available at https://www.polyu.edu.hk/ama/profile/cuijb/index.html.

not have the exact solutions of our test problems, so we display the evolution of the density from μ to ν as an indication of the quality of the approximation. Below, we present the convergence tests for Examples 4.1 and 4.2. To save on computational cost of computing the Jacobian matrix, we adopt the quasi-Newton's iteration (using the chord method) in these two examples.

Example 4.1. Here the spatial domain is the 1-torus $\mathbb{T} = [0, 1]$ subject to periodic boundary conditions. Following the approach in [29], we define a smooth function $\phi(x) = \beta sin(2\pi x)$ with $\beta = \frac{1}{32}(2\pi)^{-2}$, take initial density $\mu = \det(I - D^2\phi(x))$, and target density ν is the uniform distribution on $\mathbb{T}$. The exact initial velocity is $v^0(x) = 2\pi\beta\cos(2\pi x)$. In Tables 1 and 2, We present the error to show the linear convergence of the proposed method in space and time. We take the fixed temporal step $dt = 1/200$ in Table 1 and the fixed spatial step $dx = 1/256$ in Table 2. In this example, the single shooting method and a quasi-Newton approach (only one Jacobian matrix was computed and factored and then used across all iterations) proved to be adequate. We observe first order convergence with respect to both L^2 and sup norms, i.e., $\|\widehat{v}^0 - v^0\|_{L^\infty}, \|\widehat{v}^0 - v^0\|_{L^2}$, where $\widehat{v}$ is the initial function on the grids solved by the single shooting method, and L^∞, L^2 denote the discrete sup norm and L^2 norm, respectively.

TABLE 1
The spatial error in the velocity for Example 4.2.

dx	$\|\widehat{v}^0 - v^0\|_{L^\infty}$	$\|\widehat{v}^0 - v^0\|_{L^2}$	Iterations
1/16	$0.99074 * 10^{-3}$	$0.68763 * 10^{-3}$	4
1/32	$0.49716 * 10^{-3}$	$0.34615 * 10^{-3}$	4
1/64	$0.25731 * 10^{-3}$	$0.17476 * 10^{-3}$	4
1/128	$0.14163 * 10^{-3}$	$0.09056 * 10^{-3}$	5
1/256	$0.08756 * 10^{-3}$	$0.05118 * 10^{-3}$	10

TABLE 2
The temporal error in the velocity for Example 4.2. *Here the temporal error is computed by comparing* $\widehat{v}^0$ *with the velocity calculated by taking* $dt = \frac{1}{1024}$.

dt	$\|\widehat{v}^0 - v^0\|_{L^\infty}$	$\|\widehat{v}^0 - v^0\|_{L^2}$	Iterations
1/16	$0.24555 * 10^{-5}$	$0.16982 * 10^{-5}$	9
1/32	$0.12078 * 10^{-5}$	$0.08356 * 10^{-5}$	10
1/64	$0.05843 * 10^{-5}$	$0.04043 * 10^{-5}$	10
1/128	$0.02727 * 10^{-5}$	$0.01887 * 10^{-5}$	10
1/256	$0.01169 * 10^{-5}$	$0.00809 * 10^{-5}$	10

Example 4.2. Here the spatial domain is the 2-torus $\mathbb{T}^2 = [0, 1] \times [0, 1]$, subject to periodic boundary conditions. Following the approach in [29], we define a smooth function $\phi(x_1, x_2) = \beta \sin(2\pi x_1)\sin(2\pi x_2)$, with $\beta = \frac{1}{64}(2\pi)^{-2}$, take initial density $\mu(x_1, x_2) = \det(I - D^2\phi(x_1, x_2))$, with target density ν the uniform distribution on $\mathbb{T}^2$. In this case, the exact initial velocity can be explicitly given as

$$v^0(x_1, x_2) = 2\pi\beta(\cos(2\pi x_1)\sin(2\pi x_2), \sin(2\pi x_1)\cos(2\pi x_2)).$$

In Tables 3 and 4 we measure the approximation error of our method with respect to the spatial grid-size and temporal grid-size. In Table 3, $dt = \frac{1}{160}$ is fixed. The spatial grid size is set to be $dx = \frac{1}{128}$ in Table 4. As it turns out, this was a very easy problem to solve, because single shooting with a quasi-Newton approach solved

it adequately. There was no need to adopt a continuation strategy, and we took 160 integration steps from 0 to 1. About 90% of the computation time was spent on calculating the Jacobian at the initial guess. From Tables 3 and 4, we observe first order convergence with respect to both L^2 and sup norms. This is in agreement with the discrete scheme we used.

TABLE 3
The spatial error in the velocity for Example 4.2.

dx	$\|\widehat{v}^0 - v^0\|_{L^\infty}$	$\|\widehat{v}^0 - v^0\|_{L^2}$	Iterations
1/16	$0.45963 * 10^{-3}$	$4.21760 * 10^{-3}$	4
1/32	$0.23729 * 10^{-3}$	$0.11505 * 10^{-3}$	4
1/64	$0.12211 * 10^{-3}$	$0.05939 * 10^{-3}$	6
1/128	$0.06371 * 10^{-3}$	$0.03044 * 10^{-3}$	8

TABLE 4
The temporal error in the velocity for Example 4.2. *Here the temporal error is computed by comparing* $\widehat{v}^0$ *with the velocity calculated by taking* $dt = \frac{1}{1024}$.

dt	$\|\widehat{v}^0 - v^0\|_{L^\infty}$	$\|\widehat{v}^0 - v^0\|_{L^2}$	Iterations
1/16	$0.11940 * 10^{-5}$	$0.65367 * 10^{-5}$	8
1/32	$0.05776 * 10^{-5}$	$0.31629 * 10^{-5}$	8
1/64	$0.02695 * 10^{-5}$	$0.14760 * 10^{-5}$	8
1/128	$0.01155 * 10^{-5}$	$0.063257 * 10^{-5}$	8

4.1. 1-dimensional numerical experiments. Below we present results on 1-dimensional OT problems, with one or both densities of Gaussian types. Namely, the initial and terminal distributions μ and ν are normalizations of

$$\widehat{\mu} = \exp(-a_0(x-b_0)^2) + r_0, \quad \widehat{\nu} = \exp(-a_1(x-b_1)^2) + r_1, \tag{4.1}$$

scaled so that $\int_{\mathcal{O}} \mu dx = \int_{\mathcal{O}} \nu dx = 1$. (Here, $\mathcal{O}$ is a subinterval of the real line.)

Example 4.3. Here we look at the performance of the multiple shooting method when varying the (truncation of the real line to the) finite interval $\mathcal{O}$, and the shift number r. The parameters of initial and terminal distributions μ, ν in (4.1) are $a_0 = a_1 = 15$, $b_0 = 0.4, b_1 = 1.4$. We take $K = 60$ multiple shooting points, spatial step size $dx = 3 \times 10^{-2}$, $N = 300$ time steps per subinterval, $r_0 = r_1 = 0.0001$ in (4.1), and consider the intervals $\mathcal{O} = [0, 2]$ or $[-0.5, 2.5]$. In Figure 4.1, we plot the evolution of density. The top figures refer to $\mathcal{O} = [0, 2]$ and show distortion in the density evolution. The bottom row refers to $\mathcal{O} = [-0.5, 2.5]$ and shows that the computation is more faithful when the truncated domain is large enough.

Example 4.4. Here $\mathcal{O} = [0, 2]$, the initial distribution is the uniform distribution $\mu = \frac{1}{2}$, and the terminal distribution ν is the normalized Gaussian density as the $\hat{\nu}$ used in Example 4.3 with $a_1 = 25, b_1 = 1, r_1 = 0$. The number of multiple shooting points is $K = 60$, the space stepsize $dx = 5 \times 10^{-2}$, and we take $N = 20$ integration steps for the subinterval. Figure 4.2 shows the density evolution.

Remark 4.1. In general, we observed that when we refine the spatial step size, the number of multiple shooting subintervals must increase in order to maintain nonnegativity of the density at the temporal grids, and a successful completion of our multiple shooting method, whereas the number of integration steps on each subinterval is not

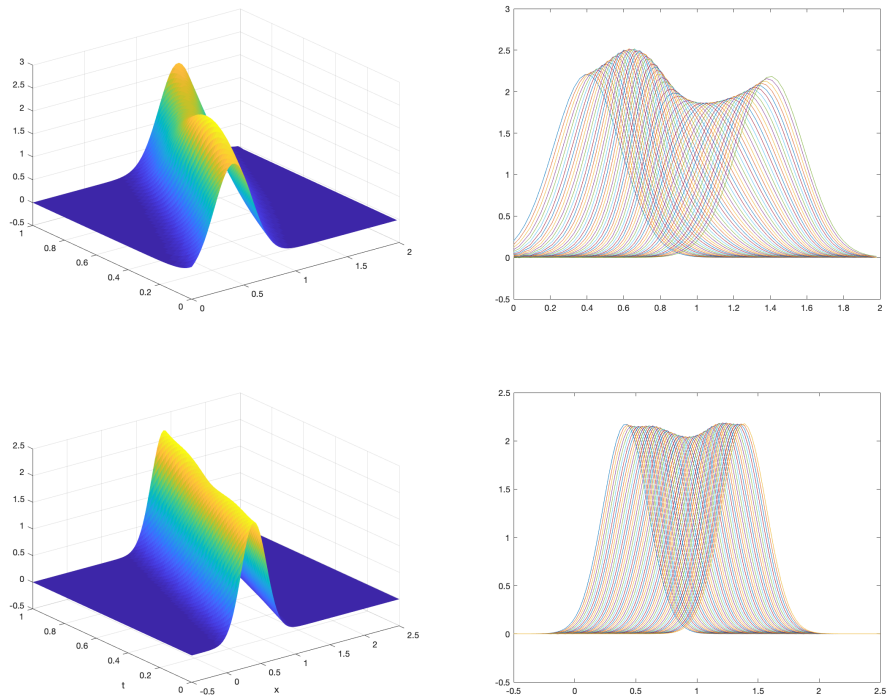

FIG. 4.1. *Example* 4.3*: evolution of* $\rho(t)$ *for truncated interval* $[0, 2]$ *(top) and* $[-0.5, 2.5]$ *(bottom).*

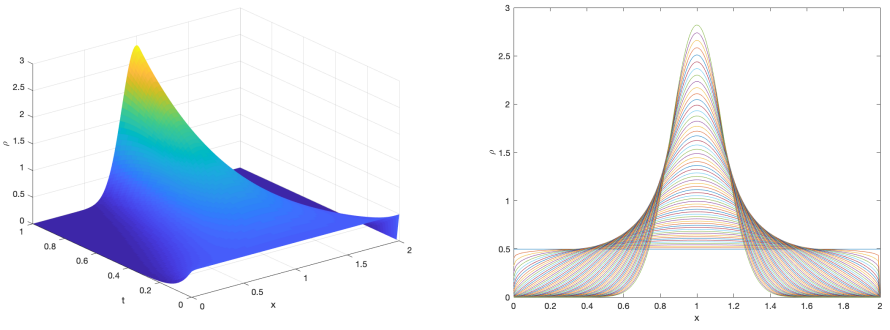

FIG. 4.2. *Evolution of probability given* μ *and* ν *in Example* 4.4.

as critical. See Table 5 for results on Example 4.4, which are typical of the general situation.

Example 4.5. This is similar to Example 4.3, but the Gaussian has a much greater variance. Let $\mathcal{O} = [-0.5, 2.5]$, $dx = 4 \times 10^{-2}$, $K = 80$, $N = 200$, and the parameters of initial and terminal Gaussian distributions μ, ν in (4.1) are $a_0 = a_1 = 50$, $b_0 = 0.4, b_1 = 1.4$, $r_0 = r_1 = 0.0001$. The evolution of the density is shown in Figure 4.3, and the sharper behavior of the density evolution with respect to Figure 4.1 is apparent.

TABLE 5
The relationship between dx, K and N in Example 4.4.

dx	K	N	Success	dx	K	N	Success
1/16	10	20	√	1/16	10	20	√
1/32	10	40	√	1/32	20	20	√
1/64	10	80	√	1/64	20	20	×
1/128	10	160	×	1/64	40	20	√
1/128	10	320	×	1/128	40	20	√

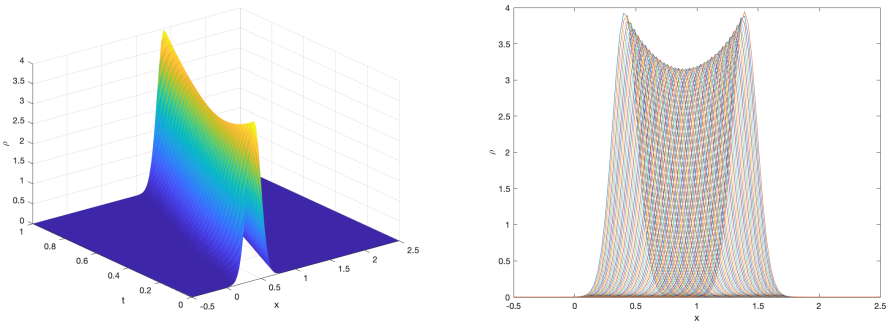

FIG. 4.3. *Evolution of probability density in Example 4.5.*

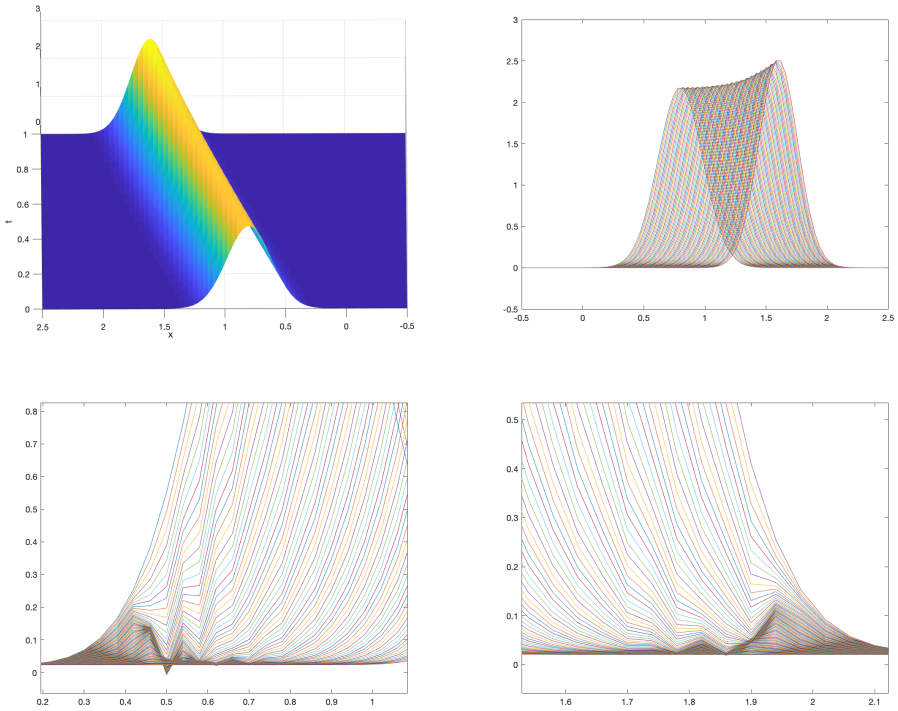

FIG. 4.4. *Evolution of probability density in Example 4.6 with $r = 0.0001$ (up) and oscillator behaviors of probability density when $r = 0.01$ (down).*

Example 4.6. This example is used to test Gaussian type distributions μ and ν with different variances. Let $\mathcal{O} = [-0.5, 2.5]$, $dx = 4 \times 10^{-2}$, $K = 80$, $N = 40$, and let the parameters of initial and terminal Gaussian distributions μ, ν be $a_0 = 15, a_1 = 10$, $b_0 = 0.8, b_1 = 1.6$, $r_0 = r_1 = 0.0001$. The evolution of the density is shown in Figure 4.4. In this problem, we also exemplify the impact of the shifting number; as can be seen in Figure 4.4, if the shifting number is not sufficiently small ($r_0 = r_1 = 0.01$, in this case), one ends up with spurious oscillatory behavior (presently, in $x = [0.4, 0.8]$ and $[1.7, 2.1]$).

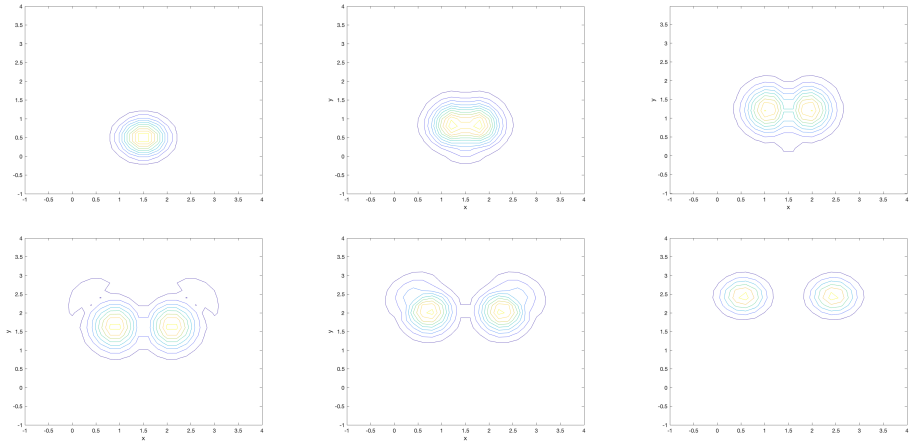

FIG. 4.5. *Example* 4.8*: contour plots of* ρ *at* $t = 0, 0.2, 0.4, 0.6, 0.8, 1$.

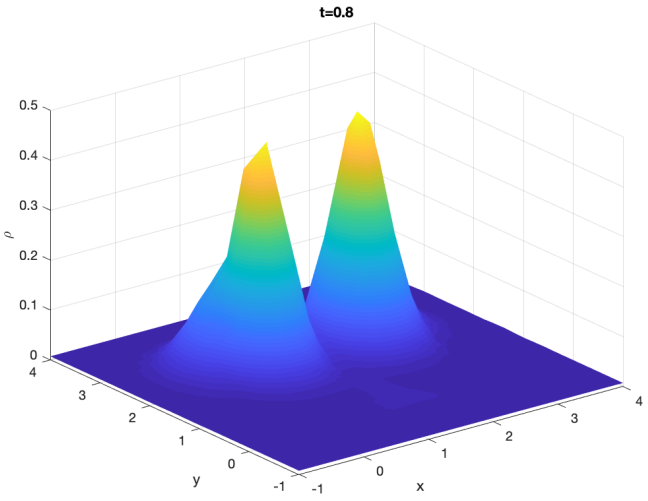

FIG. 4.6. *Example* 4.8*: surface* ρ *at* $t = 0.8$.

4.2. 2-dimensional numerical experiments. Here, we give computational results for a computational domain $\mathcal{O}$ which represents a truncation of $\mathbb{R}^2$. In Examples 4.8–4.11, we always take $K = 10$ multiple shooting subintervals, $\delta x = 0.2$ as spatial step size, and $N = 30$ integration steps on each subinterval $[t_i, t_{i+1}]$, $t_i = i/K, i = 0, \ldots, K-1$.

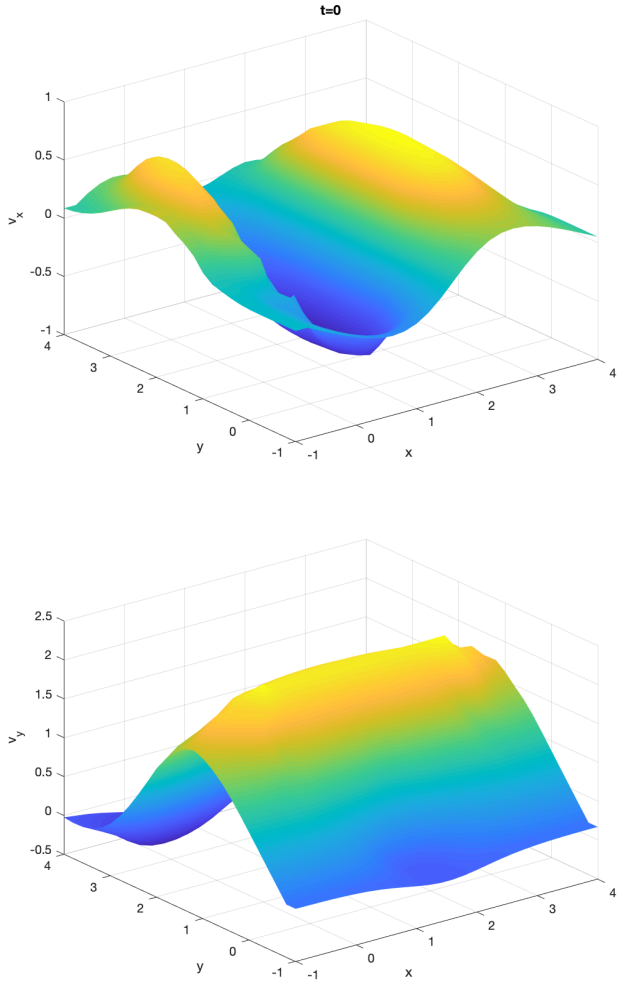

FIG. 4.7. *Example* 4.8*: two components of the initial velocity.*

In Examples 4.7 and 4.8, the initial and/or terminal distributions, μ, ν, are normalizations of Gaussian type densities, namely

$$\begin{aligned} \widehat{\mu} &= \exp(-a_0(x_2 - b_0)^2 - c_0(x_1 - d_0)^2) + r_0, \\ \widehat{\nu} &= \exp(-a_1(x_2 - b_1)^2 - c_1(x_1 - d_1)^2) + r_1. \end{aligned} \tag{4.2}$$

Example 4.7. Spatial domain is $\mathcal{O} = [-1, 3] \times [-1, 3]$. Initial and terminal densities are from (4.2) with parameters $a_0 = 2.5, a_1 = 5, b_0 = 0.5, b_1 = 1.5, c_0 = 5, c_1 =$

$10, d_0 = 0.3, d_1 = 1.3, r_0 = r_1 = 0.001$. Contour plots of the density evolution are in Figure 4.8.

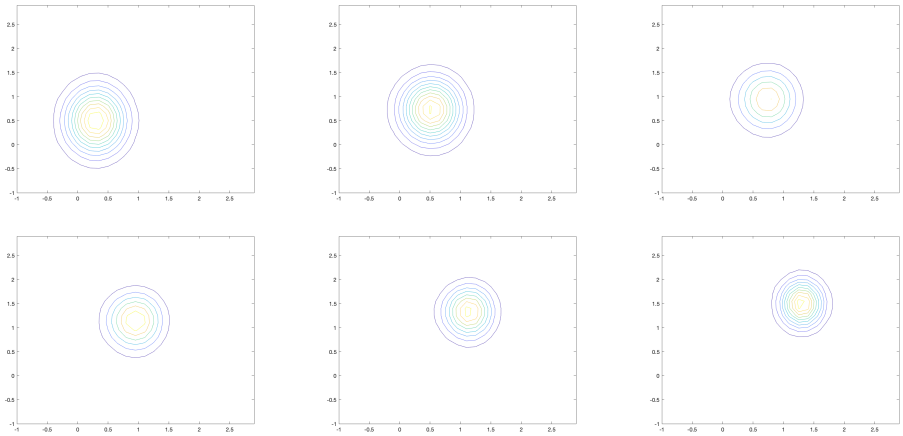

FIG. 4.8. *Example* 4.7*: contour plots of* ρ *at* $t = 0, 0.2, 0.4, 0.6, 0.8, 1$.

Example 4.8. Spatial domain is $\mathcal{O} = [-1, 4] \times [-1, 4]$. Initial density is the normalization of the Gaussian type density $\hat{\mu}$ in (4.2), with parameters $a_0 = 5, b_0 = 0.5, c_0 = 5, d_0 = 1.5,$ and $r_0 = 0.01$. The terminal distribution is the normalization of $\widehat{\nu}$ below (a two-bump Gaussian):

$$\widehat{\nu} = \exp(-5(x_2 - 2.45)^2 - 5(x_1 - 2.45)^2) + \exp(-5(x_2 - 2.45)^2 - 5(x_1 - 0.55)^2) + 0.01.$$

In Figure 4.5, we show the contour plots of the density at different times, from which the formation of the two bumps is apparent. The surfaces of the density at $t = 0.8$ and the two components of initial velocity are shown in Figures 4.6 and 4.7, respectively.

For the next set of examples, we choose the initial or terminal distributions as the normalization of the Laplace distribution. We use a_0, b_0, c_0, r_0 or a_1, b_1, c_1, r_1 to indicate the parameters of the Laplace type distribution given as

$$\begin{aligned} \widehat{\mu} &= \exp(-a_0|x_2 - b_0| - c_0|x_1 - d_0|) + r_0, \\ \widehat{\nu} &= \exp(-a_1|x_2 - b_1| - c_1|x_1 - d_1|) + r_1. \end{aligned} \tag{4.3}$$

Example 4.9. Spatial domain $\mathcal{O} = [-1, 3] \times [-1, 3]$. Initial and terminal densities are normalizations of the Laplace distributions in (4.3) with parameters $a_0 = a_1 = 5, b_0 = 0.5, b_1 = 1.5, c_0 = c_1 = 5, d_0 = 0.6, d_1 = 1.6,$ and $r_0 = r_1 = 0.001$. Contour plots of the density evolution are in Figure 4.9.

Example 4.10. Spatial domain $\mathcal{O} = [-1, 3] \times [-1, 3]$. Initial density is the uniform distribution. Terminal density is the normalization of the Laplace distribution $\hat{\nu}$ with parameters $a_1 = 10, b_1 = 1.5, c_1 = 10, d = 1.6,$ and $r = 0.01$. The contour plots of the density evolution are presented in Figure 4.10.

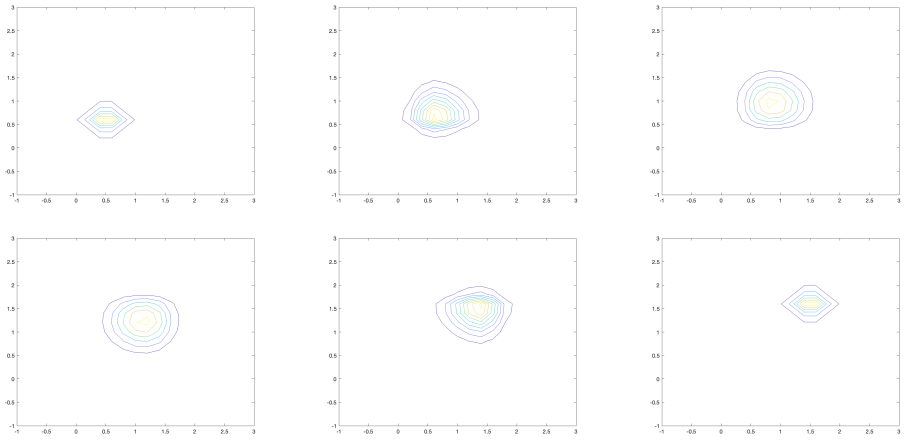

FIG. 4.9. *Example* 4.9*: contour plots of* ρ *at times* $t = 0, 0.2, 0.4, 0.6, 0.8, 1$.

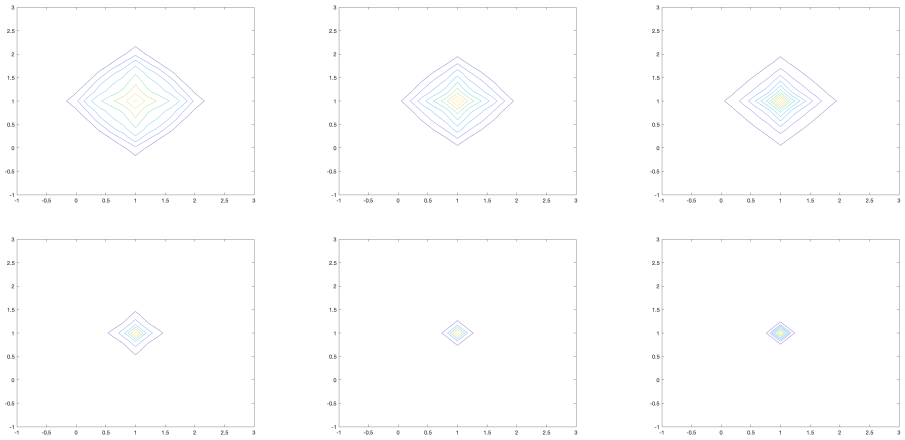

FIG. 4.10. *Example* 4.10*: contour plots of* ρ *at times* $t = 0.1, 0.3, 0.5, 0.7, 0.9, 1$.

Example 4.11. Spatial domain $\mathcal{O} = [-1, 3] \times [-1, 3]$. Initial density is the normalization of

$$\mu = (x_1 + 1)^2(x_1 - 3)^2 + (x_2 + 1)^2(x_2 - 3)^2.$$

Terminal distribution is the normalization of $\hat{\nu}$ in (4.3) with parameters $a_1 = 10, b_1 = 1.5, c_1 = 10, d_1 = 1.6,$ and $r_1 = 0.01$. The contour plots of the density evolution are presented in Figure 4.11.

Example 4.12. Spatial domain $\mathcal{O} = [x_L, x_R] \times [x_L, x_R]$, $x_L = -1, x_R = 3$. The initial density and terminal distributions are normalized Gaussian densities with parameters $a_0 = a_1 = 50, b_0 = 0.5, b_1 = 1.5, c_0 = c_1 = 50, d_0 = 0.3, d_1 = 1.3,$ and $r_1 = r_2 = 0.001$. The contour plot of the density evolution is presented in Figure 4.12.

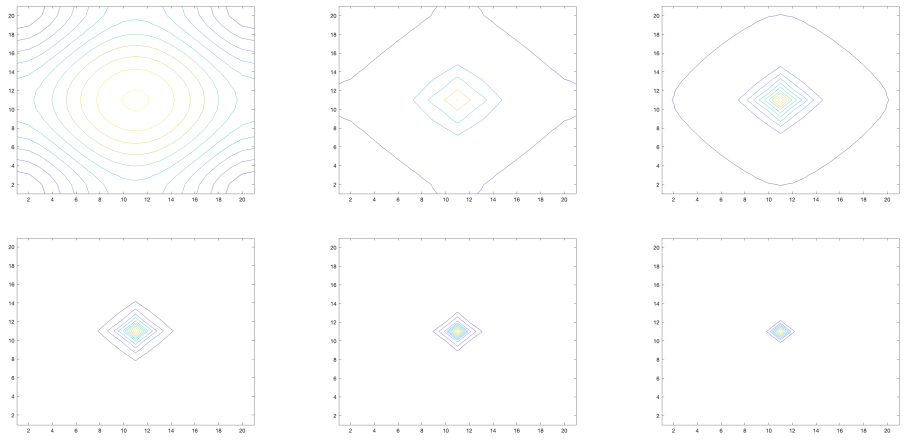

FIG. 4.11. *Example* 4.11*: contour plots of* ρ *at times* $t = 0, 0.2, 0.4, 0.6, 0.8, 1$.

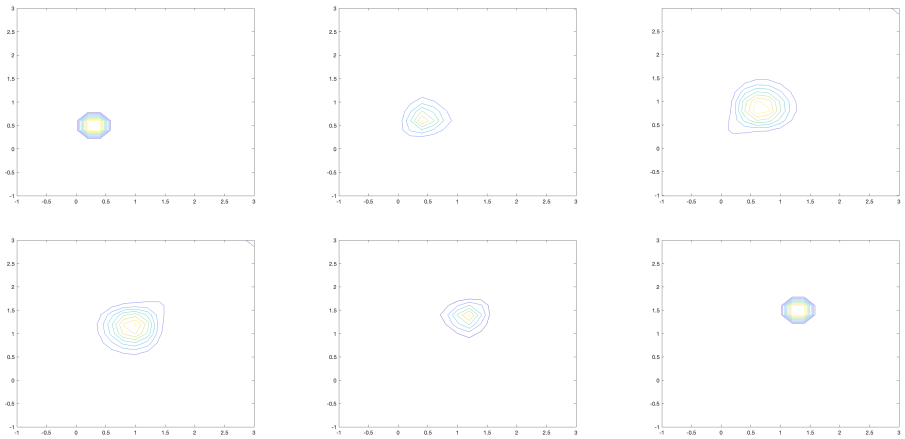

FIG. 4.12. *Example* 4.12*: contour plots of* ρ *at times* $t = 0, 0.2, 0.4, 0.6, 0.8, 1$.

5. Conclusions. In this paper, we proposed a new algorithm for the geodesic equation with L^2-Wasserstein metric on a probability set. Our algorithm is based on the Benamou–Brenier fluid-mechanics formulation of the OT problem. Namely, we view the geodesic equation as a boundary value problem with prescribed initial and terminal probability densities. To solve the BVP, we adopted the multiple shooting method and used Newton's method to solve the resulting nonlinear system. We further adopted a continuation strategy in order to enhance our ability to provide good initial guesses for Newton's method. Finally, we presented several numerical experiments on challenging problems to display the effectiveness of our algorithm.

There are many interesting questions that remain to be addressed. Surely, adaptive techniques in space and time would be very desirable, especially if one wants to extend our numerical method to the Wasserstein geodesic equations in higher dimension. The concern of truncating the spatial domain to a finite computational domain has not been addressed in our work either, but this is clearly a problem of paramount importance and will require a careful theoretical estimation of decay rates of the densities involved. We expect to tackle some of these issues in future work.

REFERENCES

[1] U. M. Ascher, R. M. Mattheij, and R. D. Russell, *Numerical Solution of Boundary Value Problems for Ordinary Differential Equations*, Prentice Hall Ser. Comput. Math., Prentice Hall, Englewood Cliffs, NJ, 1988.

[2] J. D. Benamou and Y. Brenier, *A numerical method for the optimal time-continuous mass transport problem and related problems*, in Monge Ampère equation: applications to geometry and optimization (Deerfield Beach, FL, 1997), Contemp. Math. 226, Amer. Math. Soc., Providence, RI, 1999, pp. 1–11, https://doi.org/10.1090/conm/226/03232.

[3] J. D. Benamou and Y. Brenier, *A computational fluid mechanics solution to the Monge-Kantorovich mass transfer problem*, Numer. Math., 84 (2000), pp. 375–393, https://doi.org/10.1007/s002110050002.

[4] J. D. Benamou, B. D. Froese, and A. M. Oberman, *Numerical solution of the optimal transportation problem using the Monge–Ampère equation*, J. Comput. Phys., 260 (2014), pp. 107–126, https://doi.org/10.1016/j.jcp.2013.12.015.

[5] L. A. Caffarelli, *Boundary regularity of maps with convex potentials*, Comm. Pure Appl. Math., 45 (1992), pp. 1141–1151, https://doi.org/10.1002/cpa.3160450905.

[6] Y. Chen, E. Haber, K. Yamamoto, T. T. Georgiou, and A. Tannenbaum, *An efficient algorithm for matrix-valued and vector-valued optimal mass transport*, J. Sci. Comput., 77 (2018), pp. 79–100, https://doi.org/10.1007/s10915-018-0696-8.

[7] S. Chow, L. Dieci, W. Li, and H. Zhou, *Entropy dissipation semi-discretization schemes for Fokker–Planck equations*, J. Dynam. Differential Equations, 31 (2019), pp. 765–792, https://doi.org/10.1007/s10884-018-9659-x.

[8] S. Chow, W. Li, and H. Zhou, *A discrete Schrödinger equation via optimal transport on graphs*, J. Funct. Anal., 276 (2019), pp. 2440–2469, https://doi.org/10.1016/j.jfa.2019.02.005.

[9] S. Chow, W. Li, and H. Zhou, *Wasserstein Hamiltonian flows*, J. Differential Equations, 268 (2020), pp. 1205–1219, https://doi.org/10.1016/j.jde.2019.08.046.

[10] J. Cui, L. Dieci, and H. Zhou, *Time discretizations of Wasserstein–Hamiltonian flows*, Math. Comp., 91 (2022), pp. 1019–1075, https://doi.org/10.1090/mcom/3726.

[11] J. Cui, S. Liu, and H. Zhou, *What is a stochastic Hamiltonian process on finite graph? An optimal transport answer*, J. Differential Equations, 305 (2021), pp. 428–457, https://doi.org/10.1016/j.jde.2021.10.009.

[12] M. Cuturi, *Sinkhorn Distances: Lightspeed Computation of Optimal Transport*, in Advances in Neural Information Processing Systems, C. J. C. Burges, L. Bottou, M. Welling, Z. Ghahramani, and K. Q. Weinberger, eds., Advances in Neural Information Processing Systems 26, Curran Associates, 2013, https://proceedings.neurips.cc/paper/2013/file/af21d0c97db2e27e13572cbf59eb343d-Paper.pdf.

[13] L. Dieci and J. D. Walsh, III, *The boundary method for semi-discrete optimal transport partitions and Wasserstein distance computation*, J. Comput. Appl. Math., 353 (2019),

pp. 318–344, https://doi.org/10.1016/j.cam.2018.12.034.
[14] B. D. Froese, *A numerical method for the elliptic Monge–Ampère equation with transport boundary conditions*, SIAM J. Sci. Comput., 34 (2012), pp. A1432–A1459, https://doi.org/10.1137/110822372.
[15] W. Gangbo and R. J. McCann, *The geometry of optimal transportation*, Acta Math., 177 (1996), pp. 113–161, https://doi.org/10.1007/BF02392620.
[16] D. Givoli, *Numerical Methods for Problems in Infinite Domains*, Stud. Appl. Mech. 33, Elsevier, Amsterdam, 1992.
[17] X. Gu, F. Luo, J. Sun, and S. Yau, *Variational principles for Minkowski type problems, discrete optimal transport, and discrete Monge–Ampere equations*, Asian J. Math., 20 (2016), pp. 383–398, https://doi.org/10.4310/AJM.2016.v20.n2.a7.
[18] L. V. Kantorovich, *On a problem of Monge*, J. Math. Sci., 133 (2006), 1383, https://doi.org/10.1007/s10958-006-0050-9.
[19] H. B. Keller, *Numerical Solution of Two Point Boundary Value Problems*, Regional Conference Series in Applied Mathematics 24, Society for Industrial and Applied Mathematics, Philadelphia, 1976, https://doi.org/10.1137/1.9781611970449.
[20] M. Lauriere, *Numerical Methods for Mean Field Games and Mean Field Type Control*, preprint, https://arxiv.org/abs/2106.06231, 2021.
[21] W. Li, P. Yin, and S. Osher, *Computations of optimal transport distance with Fisher information regularization*, J. Sci. Comput., 75 (2018), pp. 1581–1595, https://doi.org/10.1007/s10915-017-0599-0.
[22] L. Métivier, R. Brossie, Q. Mérigot, E. Oudet, and J. Virieux, *Measuring the misfit between seismograms using an optimal transport distance: Application to full waveform inversion*, Geophys. J. Int., 205 (2016), pp. 345–377, https://doi.org/10.1093/gji/ggw014.
[23] A. M. Oberman and Y. Ruan, *An Efficient Linear Programming Method for Optimal Transportation*, preprint, https://arxiv.org/abs/1509.03668, 2015.
[24] V. I. Oliker and L. D. Prussner, *On the numerical solution of the equation* $(\partial^2 z/\partial x^2)(\partial^2 z/\partial y^2) - ((\partial^2 z/\partial x \partial y))^2 = f$ *and its discretizations.* I, Numer. Math., 54 (1988), pp. 271–293, https://doi.org/10.1007/BF01396762.
[25] N. Papadakis, G. Peyré, and E. Oudet, *Optimal transport with proximal splitting*, SIAM J. Imaging Sci., 7 (2014), pp. 212–238, https://doi.org/10.1137/130920058.
[26] G. Peyré and M. Cuturi, *Computational Optimal Transport: With Applications to Data Science*, Foundations and Trends in Machine Learning 11, Elsevier, Amsterdam, 2019.
[27] C. R. Prins, R. Beltman, J. H. M. ten Thije Boonkkamp, W. L. Ijzerman, and T. W. Tukker, *A least-squares method for optimal transport using the Monge–Ampère equation*, SIAM J. Sci. Comput., 37 (2015), pp. B937–B961, https://doi.org/10.1137/140986414.
[28] E. K. Ryu, Y. Chen, W. Li, and S. Osher, *Vector and matrix optimal mass transport: Theory, algorithm, and applications*, SIAM J. Sci. Comput., 40 (2018), pp. A3675–A3698, https://doi.org/10.1137/17M1163396.
[29] F. Santambrogio, *Optimal Transport for Applied Mathematicians*, Calculus of Variations, PDEs, and Modeling, Progr. Nonlinear Differential Equations Appl. 87, Birkhäuser/Springer, Cham, 2015, https://doi.org/10.1007/978-3-319-20828-2.
[30] E. Tenetov, G. Wolansky, and R. Kimmel, *Fast entropic regularized optimal transport using semidiscrete cost approximation*, SIAM J. Sci. Comput., 40 (2018), pp. A3400–A3422, https://doi.org/10.1137/17M1162925.
[31] C. Villani, *Optimal Transport. Old and New*, Grundlehren Math. Wiss. 388, Springer-Verlag, Berlin, 2009, https://doi.org/10.1007/978-3-540-71050-9.
[32] H. Weller, P. Browne, C. Budd, and M. Cullen, *Mesh adaptation on the sphere using optimal transport and the numerical solution of a Monge–Ampère type equation*, J. Comput. Phys., 308 (2016), pp. 102–123, https://doi.org/10.1016/j.jcp.2015.12.018.